Zeitschrift für Kristallographie 176, 159–175 (1986)

Enstatite, $Mg_2Si_2O_6$: A neutron diffraction refinement of the crystal structure and a rigid-body analysis of the thermal vibration

Subrata Ghose

Department of Geological Sciences, University of Washington, Seattle, Washington 98195, USA

Verner Schomaker

Department of Chemistry, University of Washington, Seattle, Washington 98195, USA

and R. K. McMullan

Chemistry Department, Brookhaven National Laboratory, Upton, New York 11973, USA

Received: November 20, 1984

Enstatite / Crystal structure / Neutron diffraction / Rigid-body analysis

Abstract. Synthetic enstatite, $Mg_2Si_2O_6$, is orthorhombic, space group *Pbca*, with eight formula units per cell and lattice parameters $a = 18.235(3)$, $b = 8.818(1)$, $c = 5.179(1)$ Å at 23 °C. A least-squares structure refinement based on 1790 neutron intensity data converged with an agreement factor $R(F^2) = 0.032$, yielding Mg–O and Si–O bond lengths with standard deviations of 0.0007 and 0.0008 Å, respectively. The variations observed in the Si–O bond lengths within the silicate tetrahedra *A* and *B* are caused by the differences in primary coordination of the oxygen atoms and the proximity of the magnesium ions to the silicon atoms. The latter effect is most pronounced for the bridging bonds of tetrahedron *A*. The smallest O–Si–O angle is the result of edge-sharing by the Mg(2) octahedron and the *A* tetrahedron. An analysis of rigid-body thermal vibrations of the two crystallographically independent $[SiO_4]$ tetrahedra indicates considerable librational motion, leading to a thermal correction of apparent Si–O bond lengths as large as + 0.002 Å at room temperature.

Introduction

Enstatite is the magnesium end-member $Mg_2Si_2O_6$ of orthopyroxenes $(Mg,Fe)_2Si_2O_6$. It is a rock-forming silicate occurring in terrestrial and lunar rocks and meteorites and is considered to be an important constituent of the earth's upper mantle. Because of its geophysical importance, we have chosen it for detailed structural and lattice dynamical studies on the effects of pressure and temperature on pyroxene minerals. The enstatite structure has been refined by a number of workers using X-ray diffraction data measured under ambient laboratory pressure and temperature (Morimoto and Koto, 1969; Ghose and Wan, 1976; Hawthorne and Ito, 1977; Ghose, Wan, Ralph and McMullan, 1980; Sasaki, Fujino, Takéuchi and Sadanaga, 1980; Sasaki, Takéuchi, Fujino and Akimoto, 1982; Ohashi, 1984), as well as at 21 kbar (Ghose, et al., 1980) and (on $Mg_{0.3}Fe_{0.7}SiO_3$) up to 850°C (Smyth, 1973). We present here the results of a neutron diffraction study under ambient conditions, undertaken to obtain accurate positional and thermal vibration parameters that are unbiased by aspherical bonding electron densities of the atoms. We also present an analysis of the configurational differences in the silicate and magnesium polyhedra, together with an analysis of the rigid-body motion of the individual silicate tetrahedra of the single silicate chains. Neutron studies on two other pyroxenes, diopside, $CaMgSi_2O_6$, and spodumene, $LiAlSi_2O_6$, have been completed (Ghose and Busing, 1984).

Experimental

Crystals of orthoenstatite, $Mg_2Si_2O_6$, were obtained by the primary crystallization in the system $MgO-SiO_2-$lithium vanadomolybdate (Ito, 1975). Slow cooling (~ 1.5 deg/h) of the melt from 930°C to 650°C yielded prismatic crystals with [001] elongation, exhibiting forms {100}, {210}, and {011}. The reported composition is essentially $MgSiO_3$, with 0.17 wt% Li_2O and 0.27 wt% V_2O_5. The crystal selected for study (Table 1) was mounted within a few degrees of the c axis. Diffraction data were collected at room temperature on a 4-circle diffractometer at the Brookhaven High Flux Beam Reactor. The neutron beam, monochromatized by reflection from the 002 planes of a beryllium crystal, was of wavelength 1.0024(1) Å based on KBr ($a_o = 6.6000$ Å at 25°C).

The unit-cell parameters (Table 1) were determined by a least-squares fit of $\sin^2\theta$ values for 32 reflections distributed over the reciprocal lattice in the range $45° < 2\theta < 57°$. Intensity data were recorded for reflections $(+h,+k,+l;\ \sin\theta/\lambda \leqslant 0.80$ Å$^{-1})$ using $\theta/2\theta$ step scans over scan ranges $\Delta(2\theta) = 3.0°$ for $0° < 2\theta < 65°$ and $\Delta(2\theta) = 2.38 + 2.52 \tan\theta$, for $65° < 2\theta < 107°$. Between 60 and 88 points were sampled on the scan profiles, with counting time at each point (~ 2 s) being determined by a fixed

Table 1. Crystal data and structure refinement.

A. Crystal sample		
synthetic enstatite: $Mg_2Si_2O_6$ [a]		
principal faces	{100}, {210}, {011}	
maximum dimensions (mm)	$1.30 \times 1.00 \times 2.40$	
volume (mm^3)	2.50	
D_c ($g \cdot cm^{-3}$)	3.204	
abs. coeff. ($\mu\ cm^{-1}$)	2.40×10^{-3}	
B. Crystal data		
space group	*Pbca*	
cell content	$8[Mg_2Si_2O_6]$	
unit-cell parameters (23 °C)		
a (Å)	18.235(3)	
b (Å)	8.818(1)	
c (Å)	5.179(1)	
V (Å^3)	832.8(4)	
C. Structure refinement	extinction model [b]	
	isotropic	anisotropic
no. of observations (N_O)	1790	1790
no. of parameters (N_P)	92	97
indices of fit [c]		
$R(F^2)$	0.036	0.032
$wR(F^2)$	0.043	0.039
S	1.18	1.08
scale factor, k	3.112(5)	3.111(5)
extinction parameters ($rad^{-1} \times 10^{-5}$)		
$g_{11}(g_{iso})$, g_{22}, g_{33}	14.8(2)	8.1(8), 4.5(4), 4.4(1)
g_{12}, g_{13}, g_{23}		2.7(7), −0.3(4), 1.4(3)

[a] Ito (1975).
[b] Type I crystal with Lorentzian distribution of mosaicity (Becker and Coppens, 1974).
[c] $R(F^2) = \Sigma\Delta/\Delta F_o^2$; $wR(F^2) = \{\Sigma w\Delta^2/\Sigma F_o^4\}^{\frac{1}{2}}$; $S = \{\Sigma w\Delta^2/N_O - N_P\}^{\frac{1}{2}}$, where $\Delta = |F_o^2 - F_c^2|$.

count in the direct-beam monitor. The intensities of two reflections were remeasured at 3 h intervals and were found to be constant within 2% during the course of the experiment. For each reflection, the integrated intensity I was obtained by subtracting the background B as estimated from the first and last tenth parts of the total scan. The variance in intensity was derived from counting statistics. Absorption corrections were calculated (de Meulenaer and Tompa, 1965; Templeton and Templeton, 1973) from the measured crystal dimensions and the linear absorption coefficient μ based on the tabulated neutron (μ/ϱ) values of the International Tables for X-ray Crystallography (Vol. III, 1962). Multiple observations were averaged to give squared structure factors F_o^2 ($= I \cdot$

$\sin 2\theta$) for 1790 independent reflections, all of which were included in the refinement. None of the F_o^2 values was significantly less than zero.

Full-matrix least-squares refinement of the structure was carried out with a modified version of the computer program of Busing, Martin and Levy (1962). The quantity minimized was $\Sigma w|F_o^2 - F_c^2|^2$ with weights $w = [\sigma_c^2(F_o^2) + (0.01\,F_o^2)^2]^{-1}$, where $\sigma_c^2(F_o^2)$ is the variance from counting statistics. Neutron scattering lengths (fm), 5.380 for magnesium, 4.1491 for silicon, and 5.803 for oxygen, were taken from Koester (1977). Starting atomic positional and anisotropic thermal parameters were those determined by Ghose and Wan (1976). In the final refinement stage, secondary extinction factors (Becker and Coppens, 1974) were included as variable parameters, and refinements were carried to convergence for both isotropic and anisotropic extinction models, giving the indices of fit listed in Table 1. The latter model was taken as the better description of extinction in the crystal on the basis of Hamilton's (1964) R-factor ratio test at the 99.5% confidence level. The final atomic parameters in Table 2 are from that refinement. The maximum differences $|\Delta/\sigma|$ between the two refinements were only 0.48 and 1.92 in positional and displacement parameters, respectively. However, the U_{33} values were systematically greater, and the U_{11} and U_{22} values less, in the anisotropic refinement than in the isotropic. The extinction corrections were large: 35 reflections had correction factors ($\times F_c^2$) less than 0.75, the most severe being 0.35 for reflection 060. In the final difference map, the largest residual densities $|\Delta\varrho|$ were randomly distributed and were $\sim 1.3\%$ of ϱ at oxygen sites in the F_o synthesis. Lists of structure factors corrected for extinction were deposited[1].

Results and discussion

The crystal structure is illustrated in Figure 1, the crystallographically independent silicate chains A and B, and magnesium octahedra Mg(1) and Mg(2) in Figure 2, octahedral chains in Figure 3 and oxygen coordinations in Figure 4. The atomic notation is that of Burnham's (1967). The positional parameters in Table 2 differ very little ($\leqslant 2.1\,\sigma$) from those determined by X-ray diffraction for this synthetic enstatite (Sasaki et al., 1982), but there were significant differences in the U_{ij}'s (5.5 σ or 16%). The internuclear distances and angles relevant to this discussion are given in Table 3 and Figure 4; the standard deviations estimated from the final variance-covariance matrix are 0.0008 Å and 0.0007 Å for the Si–O and Mg–O bond lengths, respectively. Thermal motion corrections to the Si–O bond lengths up to a maximum of 0.0034 Å are estimated from an analysis (vide

[1] Additional material to this paper can be ordered from the Fachinformationszentrum Energie-Physik-Mathematik, D-7514 Eggenstein-Leopoldshafen 2, FRG. Please quote reference no. CSD 51555, the names of the authors and the title of the paper.

Table 2. Atomic parameters[a] and standard errors, in parentheses, both $\times 10^5$, for enstatite.

Atom	x	y	z	U_{11}	U_{22}	U_{33}	U_{12}	U_{13}	U_{23}
Mg(1)	37584(3)	65393(5)	86580(10)	609(17)	454(17)	371(19)	−32(15)	−57(14)	11(15)
Mg(2)	37681(3)	48693(6)	35882(10)	817(19)	664(19)	526(20)	−69(16)	−186(16)	49(16)
Si(A)	27167(3)	34166(7)	5031(12)	378(21)	373(23)	271(23)	−54(18)	34(18)	−13(20)
Si(B)	47357(3)	33732(7)	79827(12)	385(22)	321(21)	301(22)	34(18)	−22(18)	23(19)
O(1A)	18346(2)	34009(5)	3471(9)	377(16)	551(17)	488(18)	−18(13)	12(13)	19(14)
O(1B)	56231(2)	34034(5)	80017(9)	424(16)	563(16)	451(17)	6(13)	−21(14)	29(14)
O(2A)	31091(3)	50255(5)	4319(9)	732(18)	480(17)	563(19)	−207(14)	−106(15)	64(14)
O(2B)	43277(3)	48289(5)	68909(10)	737(17)	514(16)	490(18)	235(13)	−112(15)	28(15)
O(3A)	30318(3)	22259(5)	−16799(9)	560(16)	746(18)	426(18)	55(14)	−40(15)	−197(14)
O(3B)	44762(3)	19506(5)	60361(9)	579(16)	623(17)	431(16)	−74(14)	52(14)	−144(13)

[a] Anisotropic thermal parameters are of the form: $\exp[-2\pi^2(a^{*2}U_{11}h^2 + b^{*2}U_{22}k^2 + \ldots 2b^*c^*U_{23}kl)]$.

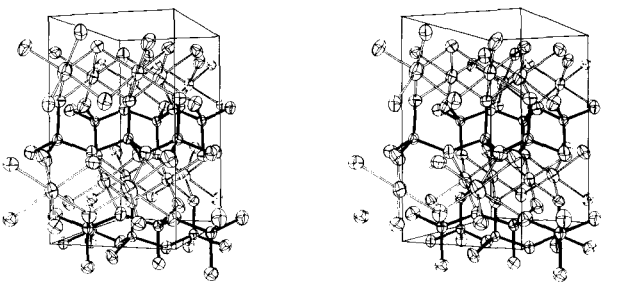

Fig. 1. The structure of enstatite in a stereoscopic view with a vertical b forward left. One-half of the cell ($0 \leqslant x \leqslant \frac{1}{2}$) is outlined. The thermal ellipsoids enclose 99.9% probability surfaces (Johnson, 1976). Shown here are two $(SiO_3)_n$ chains of each type, A and B, extending along [001] and located near $x = \frac{1}{4}$ and $x = 0$, respectively. In both chains, the bridging O(3) and terminal O(2) atoms lie roughly in the [100] planes with the Si–O(1) bonds approximately parallel to [100]. The Mg atoms between chains A and B occupy octahedral sites in $(Mg_2O_6)_n$ ribbons extending along [001].

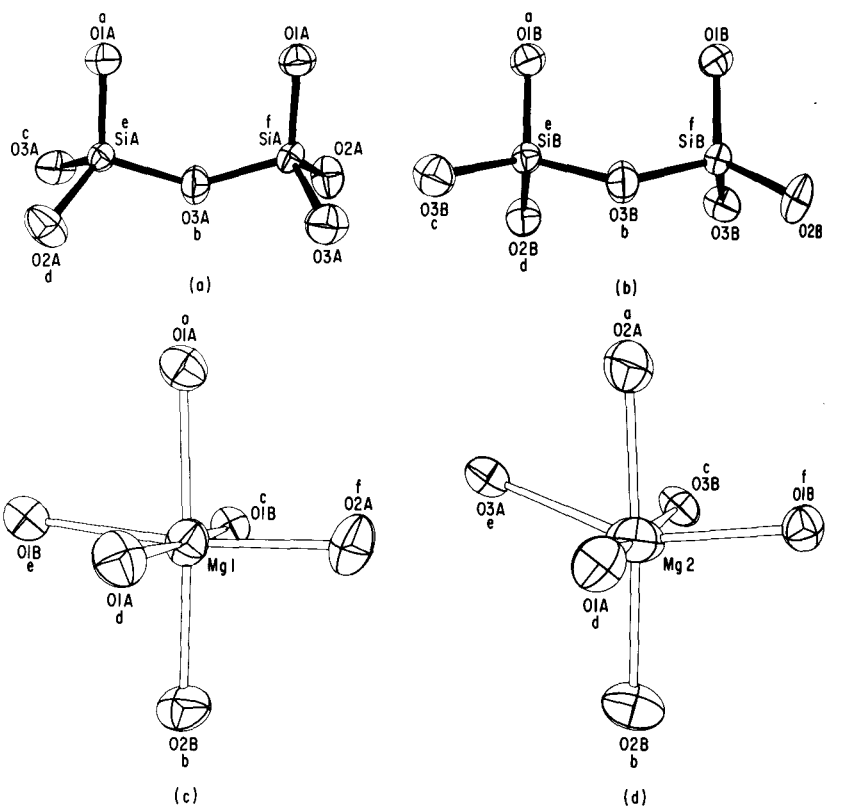

Fig. 2. The silicate chains A and B and magnesium octahedra Mg(1) and Mg(2). Lower case letters above and below the atom labels refer to symmetry operations given in Table 3. In both silicate chains, the [Si–O(3)–Si] bridges lie on the plane of the paper.

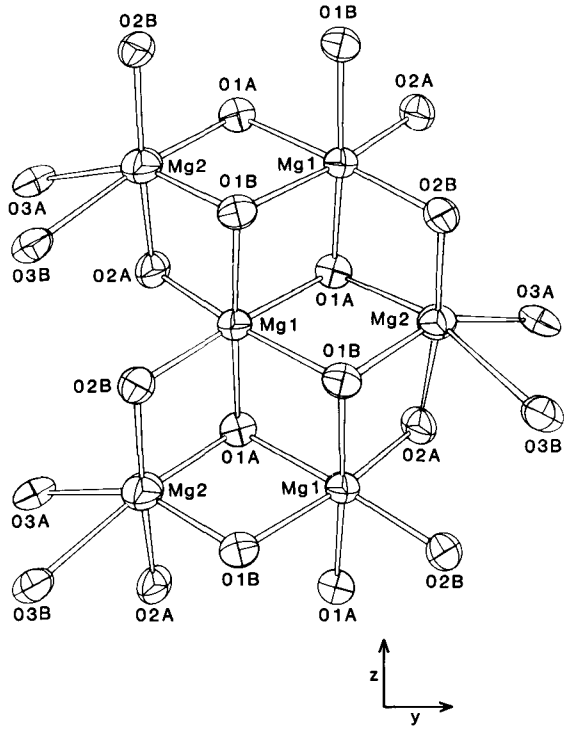

Fig. 3. Double chain of edge-sharing octahedra [Mg(1)O_6] and [Mg(2)O_6] parallel to [001].

infra) of the nuclear vibration tensors U_{ij} in Table 2. The precision of the present structure determination allows a more detailed description of the bonding geometry in enstatite than has hitherto appeared in the literature.

The silicate chains

The two [SiO_4] tetrahedra *A* and *B* each form a distinct chain along the *c* axis by sharing oxygen atoms O(3). Of the two tetrahedra, *B* is larger, and, as a consequence, the *A* chains are more extended than the *B* chains[2]. The shortest Si···Si vectors in the *A* and *B* chains are of lengths 3.053(1) Å and 3.013(1) Å, respectively, and subtend angles of 116.05(3)° and 118.52(3)°. Corresponding O(3)···O(3) distances are 2.634(1) Å and 2.765(1) Å, with the subtended angles being 158.85(3)° and 138.97(3)°.

In both chains, the bridging Si–O(3) bonds are the longest of three types, Si–O(1), Si–O(2), Si–O(3), and vary the most i.e., from

[2] The extension (or kinking) of a single silicate chain is measured by the O(3)–O(3)′–O(3)″ angle; for a fully extended chain, this angle is 180°.

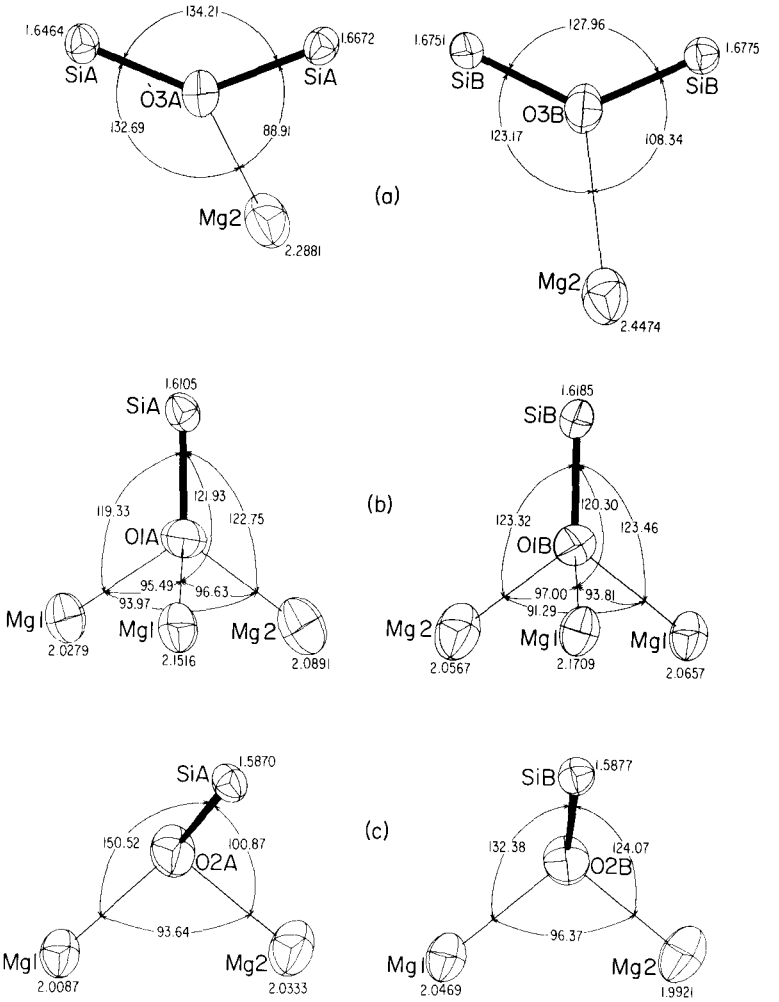

Fig. 4. The oxygen coordinations shown in order of decreasing Si–O bond lengths.

1.6464(8) Å to 1.6775(8) Å. The [Si–O(3)–Si] group of chain *A* is notably asymmetric, with bond length difference Δ(Si–O) = 0.021(1) Å, in contrast to the marginal difference, 0.002(1) Å in chain *B*. The distorted planar trigonal coordination of atoms O(3) (Fig. 4) involves Mg(2) atoms that lie off the local 2-fold axes of the *A* and *B* [Si–O(3)–Si] groups by 32.7°(*A*) and 10.9°(*B*) at Mg–O distances of 2.2881(7) Å and 2.4474(7) Å. In both groups, the longer Si–O bond lies nearer the Mg atom, and the greater difference of Δ(Si–O) in bond length occurs with the closer Mg approach distance. Such deformations suggest $Mg^{2+}-Si^{4+}$ repulsion and

Table 3. Selected distances (Å) and angles (deg)[a] in orthoenstatite at 23 °C.

A. SiO_4 tetrahedra

distance Si–O(i)		Si(A)O_4	Si(B)O_4			Si(A)O_4	Si(B)O_4
	a	1.6105	1.6185	O(i)–Si–O(j) a	b	107.98	107.34
	b	1.6464	1.6775	a	c	112.66	106.23
	c	1.6672	1.6751	a	d	117.18	117.22
	d	1.5870	1.5877	b	c	105.30	111.11
	ave.	1.6278	1.6397	b	d	113.31	104.97
				c	d	99.68	109.98
						ave. 109.35	109.48
Si–O–Si bridge				e–O(b)–f		134.21	127.96

Symmetry operations on positions (Table 2) giving sites in Si(A)O_4 and Si(B)O_4

site	atom	operation
a	O(1)	x,y,z
b	O(3)	x,y,z
c	O(3)	$x,\frac{1}{2}-y,\frac{1}{2}+z$
d	O(2)	x,y,z
e	Si	x,y,z
f	Si	$x,\frac{1}{2}-y,-\frac{1}{2}+z$

B. MgO_6 octahedra

distance Mg–O(i)		Mg(1)O_6	Mg(2)O_6	angle O(i)–Mg–O(j)		Mg(1)O_6	Mg(2)O_6
	a	2.1516	2.0333	a	b	177.22	173.84
	b	2.0469	1.9921	a	c	85.14	85.48
	c	2.0657	2.4474	a	b	93.21	89.49
	d	2.0279	2.0891	a	e	81.05	70.00
	e	2.1709	2.2881	a	f	91.48	87.02
	f	2.0087	2.0567	b	c	96.64	100.47
	ave.	2.0786	2.1511	b	d	84.93	84.73
				b	e	96.74	109.77
				b	f	90.74	94.62
				c	d	176.98	172.67
				c	e	91.69	75.36
				c	f	87.43	89.12
				e	f	172.52	152.92
				e	d	85.55	107.90
				f	d	95.15	85.29

Symmetry operation on positions (Table 2) giving sites in Mg(1)O_6 and Mg(2)O_6

Mg(1)O_6 site	atom	operation	Mg(2)O_6 site	atom	operation
a	O(1A)	$\frac{1}{2}-x,\frac{1}{2}+y,1+z$	a	O(2A)	x,y,z
b	O(2B)	x,y,z	b	O(2B)	x,y,z
c	O(1B)	$1-x,1-y,2-z$	c	O(3B)	$x,\frac{1}{2}-y,-\frac{1}{2}+z$
d	O(1A)	$\frac{1}{2}-x,1-y,\frac{1}{2}+z$	d	O(1A)	$\frac{1}{2}-x,1-y,\frac{1}{2}+z$
e	O(1B)	$1-x,\frac{1}{2}+y,\frac{3}{2}-z$	e	O(3A)	$x,\frac{1}{2}-y,\frac{1}{2}+z$
f	O(2A)	$x,y,1+z$	f	O(1B)	$1-x,1-y,1-z$

[a] Estimated standard deviations are: Mg–O: 0.0007 Å; Si–O: 0.0008 Å; O–Mg–O: 0.03°; O–Si–O: 0.04°; Si–O–Si: 0.04°.

consequent perturbation of the electron distributions in the bridging bonds by the Coulombic fields of Mg^{2+} ions at distances as great as 2.4 Å. Note that the difference between the *A*-chain bridging bonds, 0.031 Å, is as great as the average difference, 0.027 Å, between the two types of terminal bonds, Si–O(1) and Si–O(2), where O(1) is involved in a tetrahedral and O(2) in a trigonal pyramidal coordination (Fig. 4).

In the *A* and *B* tetrahedra, the terminal bonds differ by 0.023(1) Å and 0.031(1) Å, respectively, the shorter bonds, as expected, being those of 3-coordinated oxygen O(2) atoms, as opposed to the 4-coordinated oxygen O(1). The inter-chain differences in Si–O(1) and Si–O(2) bond lengths are not attributable to differences in asymmetry of local oxygen environments. The two Si–O(2) bond lengths are equal within 1 σ, while the Si–O(1) bonds differ by 0.008 Å or 8 σ. Yet, the O(1) coordinations are remarkably similar, while for O(2), there are marked differences in coordination angles Si–O(2)···Mg. Thus, the shorter and stronger terminal bonds appear to be less sensitive to local coordination differences than the longer bridging bonds.

In both chains, the largest O–Si–O angles, 117.18(3) and 117.22(3)°, are subtended by the two short, terminal Si–O bonds, while the smallest angles, 99.68(3)° and 104.97(3)°, are subtended by a bridging and a terminal bond. It should be noted that the unusually small angle of 99.68° in tetrahedron *A* involves the O(3)–O(2) edge, which is shared with the Mg(2) octahedron (Fig. 1).

The two Si–O(3)–Si angles are distinctly different [134.21(3)° in *A* and 127.96(3)° in *B*] and are both somewhat less than the average of 144° given for related silicates (Tossell and Gibbs, 1978). The wider angle goes with the shorter, bridging Si–O bonds, consistent with previous observations on the [Si–O–Si] bridging groups (see Gibbs, 1982) and quantum mechanical calculations on the $H_6Si_2O_7$ molecule (Newton and Gibbs, 1980).

The MgO_6 octahedra

The Mg(1) octahedra form the backbone of the zigzag double octahedral strip of Mg_2O_6 extending along the *c* axis (Fig. 3). These octahedra are fairly regular with an average Mg–O distance of 2.08 ± 0.07 Å and maximum angle distortion of 9.0°. On the other hand, the Mg(2) octahedra, which link the two tetrahedra–octahedra–tetrahedra (T–O–T) strips together are highly distorted (Figs. 2 and 3) with two unusually long bonds, Mg(2)–O(3A) = 2.2881(7) Å and Mg(2)–O(3B) = 2.4474(7) Å. In addition, the O(3A) bond angles are irregular, evidently as a result of the O(3A)···O(2A) edge-sharing with the *A* tetrahedron. The inequality of the two Mg(2)–O(3) bonds from each other is in contrast with the situation found in the high temperature $C2/c$ phase of $(Mg,Fe)_2Si_2O_6$ (Smyth, 1974),

where these two bonds are equal. The present bonding situation is comparable to the effectively five-fold coordination of magnesium-rich M(4) polyhedron in ferromagnesian ampliboles, *viz*, anthophyllite and primitive cummingtonite, $(Mg,Fe)_7Si_8O_{22}(OH)_2$ (Ghose, 1982). It should be noted that these two long Mg(2)–O(3) bonds, particularly the longer one, are very sensitive to temperature, pressure and chemical substitution (Smyth, 1973; Ralph and Ghose, 1980; Ghose, 1982). Thus, a precise determination of these bond length values in enstatite is important for estimating the amount of substituting cations, such as Al in aluminous orthopyroxenes, which cannot be easily distinguished from Mg by X-ray diffraction (Ganguly and Ghose, 1979).

Anisotropic thermal motion

The nuclear U_{ij} parameters provide a realistic pattern of r.m.s. displacements (mainly thermal vibrations) consistent with the bonding environments in the crystal. For chemically equivalent atoms of the two silicate chains, the r.m.s. amplitudes of vibration along respective principal axes of the thermal ellipsoids (Table 4A) are equal within 2 σ, except for bridging atoms O(3A) and O(3B), which have distinctly different bonding environments. As expected, atoms O(2) and O(3), in trigonal sites, show greater thermal anisotropy than do atoms Si and O(1), with their more nearly isotropic tetrahedral configurations. Likewise, the anisotropy and amplitudes of vibration are greater for Mg(2), in the more distorted and larger octahedron, than for Mg(1). In the silicate chains, the r.m.s. displacements of Si and O along respective Si–O bonds (Table 4B) are nearly equal, in accord with the great strength of these bonds. (This correlated motion is a necessary, but not a sufficient, condition that the $[SiO_4]$ tetrahedra vibrate as rigid groups.) The vibrational motion of adjacent Mg and O atoms also appear to be coupled in the $[Mg(1)O_6]$ group, though to a lesser extent, and, to a much lesser extent in the larger $[Mg(2)O_6]$ group.

In the following discussion, we present a rigid-body analysis of the thermal vibrations of the two distinct silicate tetrahedra with attempts to account for their internal vibrations. This analysis is not concerned with correlations between the motion of a particular $[SiO_4]$ group and the atoms of the rest of the crystal, nor does it account for the forces involved, e.g., the Coulombic interaction with the Mg^{2+} ions.

Rigid-body analysis of the thermal vibration of the silicate tetrahedra and the thermal correction of the Si – O bond lengths

In a silicate such as enstatite, the interatomic forces within a tetrahedral $[SiO_4]$ group are much stronger than the forces between such groups (except, of course, for the forces that link the tetrahedra into chains). In any

case, if there is appreciable vibration, bond lengths may require correction: the distance between the average positions of two atoms on a crystal structure, as found by diffraction, is shorter than the average distance between these atoms to an extent that depends on the mean square *relative transverse* displacements of the atoms (Cruickshank, 1956; Busing and Levy, 1964). These relative displacements are not fully defined by the

Table 4. Amplitude and directions of nuclear thermal motion at 23 °C.

A. R.m.s. displacements and orientations of principal axes of thermal ellipsoids relative to crystal axes *a*, *b*, *c*

Atom	Principal axes	R.m.s.d.	Angles with crystal axes[a]		
			a	*b*	*c*
Mg(1)	1	0.060(1) Å	78(3)°	92(9)°	13(3)°
	2	0.067(1)	101(5)	169(5)	90(9)
	3	0.080(1)	16(4)	101(4)	105(3)
Mg(2)	1	0.066(1)	65(2)	94(4)	25(2)
	2	0.080(1)	107(3)	163(3)	86(4)
	3	0.097(1)	31(2)	107(3)	115(2)
Si(A)	1	0.051(2)	105(11)	91(13)	15(11)
	2	0.057(2)	128(10)	140(8)	100(16)
	3	0.066(2)	42(8)	130(8)	79(6)
Si(B)	1	0.052(2)	72(8)	128(15)	43(16)
	2	0.057(2)	80(13)	136(16)	133(16)
	3	0.064(2)	21(9)	70(11)	97(11)
O(1A)	1	0.062(1)	7(5)	84(4)	94(7)
	2	0.069(1)	93(7)	105(10)	164(10)
	3	0.075(1)	97(4)	17(10)	105(10)
O(1B)	1	0.064(1)	35(15)	98(6)	57(15)
	2	0.068(1)	125(15)	101(7)	37(15)
	3	0.075(1)	90(6)	14(6)	76(6)
O(2A)	1	0.060(1)	61(2)	29(2)	92(5)
	2	0.072(1)	109(3)	82(5)	160(2)
	3	0.095(1)	35(2)	117(1)	110(2)
O(2B)	1	0.057(1)	58(1)	135(3)	62(4)
	2	0.072(1)	85(3)	120(3)	150(4)
	3	0.095(1)	32(1)	60(2)	101(2)
O(3A)	1	0.058(1)	87(4)	65(2)	26(2)
	2	0.074(1)	167(3)	77(3)	93(3)
	3	0.093(1)	77(2)	29(2)	115(1)
O(3B)	1	0.059(1)	93(4)	63(3)	28(2)
	2	0.073(1)	151(3)	116(4)	80(4)
	3	0.087(1)	62(3)	140(3)	65(2)

Table 4. (Continued)

B. R.m.s. components of thermal motion along Si–O and Mg–O bonds: for atom *X* in the direction of atom *Y*

	X *Y*	*X* *Y*		*X* *Y*	*X* *Y*
	O–Si(A)	Si(A)–O		O–Si(B)	Si(B)–O
O(1A)	0.062(1) Å	0.062(2) Å	O(1B)	0.065(1) Å	0.062(2) Å
O(2A)	0.060(1)	0.057(2)	O(2B)	0.057(1)	0.053(2)
O(3A)	0.063(1)	0.057(2)	O(3B)	0.064(1)	0.059(2)
O(3A)′	0.059(1)	0.058(2)	O(3B)′	0.062(1)	0.056(2)
ave.	0.061	0.059	ave.	0.062	0.058
[b]	$S = 1.01$			$S = 1.37$	
	O–Mg(1)	Mg(1)–O		O–Mg(2)	Mg(2)–O
O(1A)	0.067(1)	0.062(1)	O(1A)	0.072(1)	0.080(1)
O(1A)	0.069(1)	0.073(1)	O(2A)	0.073(1)	0.067(1)
O(2A)	0.066(1)	0.070(1)	O(3A)	0.080(1)	0.080(1)
O(1B)	0.073(1)	0.069(1)	O(1B)	0.071(1)	0.083(1)
O(1B)	0.065(1)	0.062(1)	O(2B)	0.067(1)	0.066(1)
O(2B)	0.068(1)	0.073(1)	O(3B)	0.076(1)	0.092(1)
ave.	0.068	0.068	ave.	0.073	0.078
	$S = 1.62$			$S = 3.50$	

[a] Note that the largest uncertainties are in orientations for Si and O(1) i.e., for the most nearly isotropic ellipsoids.

[b] $S = \left[\sum^{n}(\Delta/\sigma)^2\right]^{\frac{1}{2}}/(n-1)$, where Δ is the difference between the r.m.s. displacements of atoms *X* and *Y* along the bond direction.

diffraction data, and can hardly be evaluated reliably without a full consideration of all modes of vibration of the crystal, which is very difficult or impossible at this point. However, it is often useful to describe the mean square displacement (or vibrations) of the atoms in a group as arising mainly from rigid motion (translations and librations) of the group and only to a minor extent from (internal) vibrations, i.e., in an $[SiO_4]$ group the Si–O bond stretchings and angle bendings. In some degree of approximation, external (lattice) modes of vibration of the crystal correspond to these translations and librations, and internal modes to the distortions. The utility of this treatment depends on the extent to which the internal displacements are indeed small or are subject to independent estimation.

With the rigid-body model, the U_{ij}'s do afford estimates of the amount of libration and hence the relative transverse amplitudes and, finally, corrections for bond-length foreshortening. Even at room temperature, these corrections for enstatite amount to + 0.002 Å, considerably more than the standard deviation (± 0.0008 Å). This approach also yields an estimate of

Table 5. Enstatite, Si–O bond lengths (Å): I, uncorrected; II, corrected for rigid-body [SiO_4] libration; III, corrected for libration with allowance for internal vibrations.

	I	II	III
Si(A)–O(1A)	1.6105	1.6118	1.6132
–O(2A)	1.5870	1.5887	1.5901
–O(3A)	1.6464	1.6484	1.6498
–O(3A)′	1.6672	1.6686	1.6700
Si(B)–O(1B)	1.6185	1.6198	1.6212
–O(2B)	1.5877	1.5891	1.5905
–O(3B)	1.6775	1.6787	1.6801
–O(3B)′	1.6751	1.6763	1.6777

Table 6. Rigid-body libration parameters of silicate tetrahedra in enstatite.

		Deg.[2]	Direction cosines with respect to			QM frq. cm^{-1}
			+a	+b	+c	
Si(A) tetrahedron						
L eigen values	L_1	6.47	0.851	−0.002	0.524	224
	L_2	2.38	0.420	−0.595	−0.648	292
	L_3	2.19	0.314	0.803	−0.506	315
WRMSΔU[a]		0.002				
Si(B) tetrahedron						
L eigen values	L_1	4.72	0.056	−0.293	−0.954	264
	L_2	3.26	−0.960	0.245	−0.132	260
	L_3	1.13	0.273	0.924	−0.268	483
WRMSΔU		0.0003				

[a] $\text{WRMS}\Delta U \equiv \left(\frac{\Sigma w(u_{obs}-u_{calc})^2}{\Sigma w}\right)^{\frac{1}{2}}$, a weighted sum over components and atoms.

the principal librational frequencies, which perhaps can be correlated with the low frequency phonon modes determined from Raman and IR measurements.

Using the formalism developed by Schomaker and Trueblood (1968), we have carried out such an analysis with the program THMB (Trueblood, 1978) for the two crystallographically distinct silicate tetrahedra, *A* and *B*, with the results listed in Tables 5 and 6. Both tetrahedra passed the rigidity test, except the O(3)–O(3)′ edges, which appear to be fairly soft. The librational motion is larger for *A*, with the greatest principal axis of libration parallel to O(1A)–O(3A), than for *B*, with the greatest libration axis parallel to O(3B)–O(3B)′. The greater degree of librational motion of *A*

is consistent with its smaller size and the fact that the Si(A) chain is more extended than the Si(B) chain. The axis of greatest libration for *A* can be resolved into two perpendicular components roughly parallel to Si(A)–O(1A) and to O(3A)–O(3A)′, the former being normal to the plane of the silicate chains, i.e., the (100) plane and the latter parallel to the direction of chain extension, i.e., the [001] axis. Note, however, that chain *B*, the more kinked of the two, extends or contracts more than chain *A* with changes of temperature (Smyth, 1973) or pressure (Ralph and Ghose, 1980).

The normal frequencies of libration of the silicate tetrahedra as provided by THMB fall in the range $200-500\ cm^{-1}$. The Raman spectrum of a polished and oriented single crystal of enstatite, $Mg_{0.8}Fe_{0.2}SiO_3$, has a number of weak peaks in the range (White, 1983), and some of these (e.g., 188, 234, 268, 293, 463 cm^{-1}) may very well be of essentially librational origin. However, it must be said that the THMB normal-mode estimates may be uncertain, since they depend on several assumptions, including the assumption that libration and translation are not coupled.

The thermal corrections to the Si–O bond lengths (Table 5) are significant even at room temperature, the largest amounting to about + 0.0020 Å. At higher temperature, these corrections will increase, which will counteract the apparent shortening of the Si–O bonds in orthopyroxene previously reported (Smyth, 1973).

We have also tried to estimate the contributions of the $[SiO_4]$ internal vibration by subtracting from the U_{ij}'s the mean square amplitudes due to the nine internal vibrations as calculated for a symmetrical (T_d) free silicate group with frequencies 800 cm^{-1} for $\nu_1(A_1)$, pure stretching, 400 cm^{-1} for $\nu_2(E_2)$, pure bending, and 1000 cm^{-1} and 600 cm^{-1} for the two F_2 vibrations, these latter being further assumed to be pure stretching and pure bending, respectively. The corresponding mean square amplitudes are very nearly isotropic for both silicon and the oxygens. The corrected coordinates from a subsequent THMB calculation led to Si–O distances greater than those from the original coordinates by amounts ranging from 0.0012 Å to 0.0020 Å, hardly different than before. But one must now add the correction for the perpendicular components of the internal vibrations, 0.0014 Å (the same for each Si–O by the assumed T_d vibrational symmetry); the corrected distances now greater than the original distances by amounts ranging from 0.0026 to 0.0034 Å, are probably the best of the three sets despite the great uncertainties of the internal-vibration model. The new eigenvalues average 12(4)% smaller than those given in Table 6; the estimated frequencies are correspondingly higher and the fit of calculated to observed U_{ij} values is not improved.

We have also run THMB for the $Mg(1)O_6$ and $Mg(2)O_6$ octahedra. Whereas the Mg(1) octahedra passes the THMB rigidity test quite well, the Mg(2) octahedron does not. This is consistent with the high degree of distortion of the Mg(2) octahedron. The librational motion of the Mg(1)

octahedron is small and the corresponding corrections to the Mg(1)–O bond lengths are negligible.

Acknowledgements. We are indebted to the late Dr. Jun Ito for the donation of synthetic enstatite crystals. The neutron data collection and much of the computations were carried out at Brookhaven National Laboratory under contract with the US Department of Energy (DE-AC02-76CH00016) and supported by its Office of Basic Energy Sciences. S. Ghose acknowledges support by NSF grants EAR 79-04886 and EAR 82-06526.

References

Becker, P. J., Coppens, P.: Extinction within the limit of validity of the Darwin transfer equations. General formalisms for primary and secondary extinctions and their application to spherical crystals. Acta Crystallogr. **A30**, 129–147 (1974)

Burnham, C. W.: Ferrosilite. Carnegie Inst. Wash. Year Book. **65**, 285–290 (1967)

Busing, W. R., Martin, K. O., Levy, H. A.: ORFLS, a FORTRAN crystallographic least-squares program. US Atomic Energy Commission Report No ORNL-TM-305 (1962)

Busing, W. R., Levy, H. A.: The effect of thermal motion on the estimation of bond lengths from diffraction measurements. Acta Crystallogr. **17**, 142–146 (1964)

Cruickshank, D. W. J.: Errors in bond lengths due to rotational oscillations of molecules. Acta Crystallogr. **9**, 757–758 (1956)

Ganguly, J., Ghose, S.: Aluminous orthopyroxene: order-disorder, thermodynamic properties and petrologic implications. Contrib. Mineral. Petrol. **69**, 375–385 (1979)

Ghose, S.: Mg–Fe order-disorder in ferromagnesian silicates I. Crystal chemistry. In: *Advances in Physical Geochemistry* (Ed. S. K. Saxena) Vol. 2, 3–57, Springer-Verlag (1982)

Ghose, S., Wan, C.: Site preference of Cu^{2+}-ions in enstatite and the refinement of the crystal structure of pure enstatite (abstract). Trans. Am. Geophys. Union **57**, 337 (1976)

Ghose, S., Wan, C., Ralph, R. L., McMullan, R. K.: Enstatite, $Mg_2Si_2O_6$: charge density distribution by X-ray and neutron diffraction and the compressibility of the crystal structure at 21 kbar (abstract). Collected Abstracts, International Mineralogical Association Meeting, 48–49 (1980)

Ghose, S., Busing, W. R.: in preparation (1984)

Gibbs, G. V.: Molecules as models for bonding in silicates. Am. Mineral. **67**, 421–450 (1982)

Hamilton, W. C.: *Statistics in Physical Sciences*, pp. 216–222. New York: The Ronald Press Company 1964

Hawthorne, F. C., Ito, J.: Synthesis and crystal-structure refinement of transition-metal orthopyroxenes 1: orthoenstatites and (Mg, Mn, Co) orthopyroxenes. Can. Mineral. **15**, 321–338 (1977)

International Tables for X-ray Crystallography, Vol. III, 197, Birmingham, Kynoch Press (1962)

Ito, J.: High temperature solvent growth of enstatite, $MgSiO_3$ in air. Geophys. Res. Lett. **2**, 533–535 (1975)

Johnson, C. K.: ORTEP: A FORTRAN thermal-ellipsoid plot program for crystal structure illustration. Report ORNL-5138, Oak Ridge National Laboratory, Tennessee (1976)

Koester, L.: *Neutron Physics*. In: Springer Tracts in Modern Physics (Ed. G. Höhler) p. 36–39. Berlin: Springer-Verlag 1977

Meulenaer, J. de, Tompa, H.: The absorption correction in crystal structure analysis. Acta Crystallogr. **19**, 1014–1018 (1965)

Morimoto, N., Koto, K.: The crystal structure of orthoenstatite. Z. Kristallogr. **129**, 65–83 (1969)

Newton, M. D., Gibbs, G. V.: *Ab Initio* calculated geometries and charge distributions for H_4SiO_4 and $H_6Si_2O_7$ compared with experimental values for silicates and siloxanes. Phys. Chem. Minerals **6**, 221–246 (1980)

Ohashi, Y.: Polysynthetically twinned structures of enstatite and wollastonite. Phys. Chem. Minerals **10**, 217–229 (1984)

Ralph, R. L., Ghose, S.: Enstatite, $Mg_2Si_2O_6$: compressibility and crystal structure at 21 kbar (abstract). EOS, Trans. Am. Geophys. Union **61**, 409 (1980)

Sasaki, S., Fujino, K., Takéuchi, Y., Sadanaga, R.: On the estimation of atomic charges by X-ray methods for some oxides and silicates. Acta Crystallogr. **A36**, 904–915 (1980)

Sasaki, S., Takéuchi, Y., Fujino, K., Akimoto, S.: Electron-density distributions of three orthopyroxenes. Z. Kristallogr. **158**, 279–297 (1982)

Schomaker, V., Trueblood, K. N.: On the rigid-body motion of molecules in crystals. Acta Crystallogr. **B24**, 63–76 (1968)

Smyth, J. R.: An orthopyroxene structure up to 850°C. Am. Mineral. **58**, 636–648 (1973)

Smyth, J. R.: The high temperature crystal chemistry of clinohyperstrene. Am. Mineral. **59**, 1069–1082 (1974)

Templeton, L. K., Templeton, D. H.: Calculation of the absorption correction by the analytical method. (Abstract) American Crystallographic Association Meeting, Storrs, Conn., p. 143 (1973)

Tossell, J. A., Gibbs, G. V.: The use of molecular-orbital calculations on model systems for the prediction of bridging-bond-angle variations in siloxanes, silicates, silicon nitrides and silicon sulfides. Acta Crystallogr. **A34**, 463–472 (1978)

Trueblood, K. N.: Analysis of molecular motion with allowance for intermolecular torsion. Acta Crystallogr. **A34**, 950–954 (1978)

White, W. B., personal communication (1983)